The
University
Of
Sheffield.

This is a repository copy of *Effects of hydrogen relative humidity on the performance of an air-breathing PEM fuel cell : a numerical study*.

White Rose Research Online URL for this paper:
http://eprints.whiterose.ac.uk/144415/

Version: Accepted Version

Article:

eprints@whiterose.ac.uk
https://eprints.whiterose.ac.uk/

Title Page

Title

Effects of hydrogen relative humidity on the performance of an air-breathing PEM fuel cell: a numerical study

Authors

Z.X. Chen, D.B. Ingham, M.S. Ismail, L. Ma, K.J. Hughes [*], and M. Pourkashanian

Energy 2050, Department of Mechanical Engineering, University of Sheffield, Sheffield S3 7RD, UK.

[*] Corresponding author: Tel: + 44 (0) 114 21 57214

Email address: K.J.Hughes@sheffield.ac.uk (K.J. Hughes)

Abstract

Purpose – The purpose of this study is to investigate the effects of hydrogen humidity on the performance of air-breathing PEM fuel cells.

Design/methodology/approach – An efficient mathematical model for air-breathing proton exchange membrane (PEM) fuel cells has been built in Matlab. The sensitivity of the fuel cell performance to the heat transfer coefficient is investigated first. The effect of hydrogen humidity is also studied. In addition, under different hydrogen humidities, the most appropriate thickness of the gas diffusion layer (GDL) is investigated.

Findings – The heat transfer coefficient dictates the performance limiting mode of the air-breathing PEM fuel cell, the modelled air-breathing fuel cell is limited by the dry-out of the membrane at high current densities. The performance of the fuel cell is mainly influenced by the hydrogen humidity. Besides, an optimal cathode GDL and relatively thinner anode GDL are favoured in order to achieve a good performance of the fuel cell.

Practical implications – The current study improves the understanding of the effect of the hydrogen humidity in air-breathing fuel cells, and this new model can be used to investigate different component properties in real designs.

Original/value – The hydrogen relative humidity and the GDL thickness can be controlled in order to improve the performance of air-breathing fuel cells.

Keywords Numerical model; Air-breathing PEM fuel cells; Relative humidity; Water management

Nomenclature

a	water activity	-
A	active area of fuel cell	m^2
C	molar concentration	$mol\ m^{-3}$
D	diffusion coefficient	$m^2\ s^{-1}$
e	emissivity	-
E	cell voltage	V
E_o	thermodynamic equilibrium voltage	V
F	Faraday's constant	$C\ mol^{-1}$
g	magnitude of gravitational acceleration	$m\ s^{-2}$
h	hear transfer coefficient	$W\ m^{-2}\ K^{-1}$
h_m	mass transfer coefficient	$mol\ s^{-1}$
H	enthalpy	$kJ\ mol^{-1}$
I	current density	$A\ m^{-2}$
I_o	exchange current density	$A\ m^{-2}$
j_w	water flux	$mol\ m^{-2}\ s^{-1}$
k	thermal conductivity	$W\ m^{-1}\ K^{-1}$
L	characteristic length	m
M	molecular weight	$g\ mol^{-1}$
n	number of electrons per mole of species of interest	$electron\ mol^{-1}$
n_d	electro-osmotic coefficient	-
N	molar flux	$mol\ m^{-2}\ s^{-1}$
Nu	Nusselt number	-
P	pressure	Pa
P_{sat}	saturation pressure of water vapour	Pa
q	heat flux	$W\ m^{-2}$
R	universal gas constant	$J\ mol^{-1}\ K^{-1}$
Ra	Rayleigh number	-
RH	relative humidity	%

R_{elec}	electrical resistance	Ω
R_{mem}	ionic resistance of membrane	Ω
S	entropy	J mol^{-1} K^{-1}
Sh	Sherwood number	-
T	temperature	K
x	molar fraction	-

Greek symbols

α	thermal diffusivity	m^2 s^{-1}
α_{ch}	charge transfer coefficient	-
β	thermal expansion coefficient	K^{-1}
β_m	volumetric expansion coefficient	-
δ	thickness	m
ε	porosity	-
η_{act}	activation loss	V
η_{ohmic}	ohmic loss	V
λ	water content	-
ν	kinematic viscosity	m^2 s^{-1}
σ_{Bolt}	Stephan-Boltzmann constant	W m^{-2} K^{-4}
σ_{mem}	ionic conductivity	S m^{-1}

1. Introduction

Air-breathing fuel cells have attracted considerable attention for replacing batteries in some portable devices, such as laptops and smartphones (Carcadea et al., 2007; Ismail et al., 2016, 2015; Li and Ake Sunden, 2018; Mahmud Hasan et al., 2011; O'Hayre et al., 2007). Unlike conventional PEM fuel cells, mass and heat transfer at the cathode side is governed by natural convection in the air-breathing PEM fuel cells, thus simplifying the fuel cell system. Namely, the air-breathing fuel cell system normally consists of only the fuel cell (or the fuel cell stack) and a storage device for hydrogen. However, this simplification causes a rather low performance when compared with that of the conventional fuel cells and this is due to the low mass and heat transfer coefficients at the open cathode of the air-breathing PEM fuel cell (Schmitz et al., 2006).

In order to improve the performance of air-breathing PEM fuel cells, there have been a number of both modelling and experimental investigations to examine the effects of some of the geometrical and operational parameters on the performance of air-breathing fuel cells (Coz et al., 2016; Fabian et al., 2010; Ismail et al., 2013; Jeong et al., 2006), e.g. ambient conditions and open ratios of the cathode GDL.

Water management is an important issue in PEM fuel cells and this is closely related to both flooding at the cathode and dry-out of the membrane. The flooding at the cathode significantly increases the concentration losses because it hinders the transport of oxygen from the ambient (in the case of the air-breathing mode of operation) or the flow channel to the catalyst layer, while the dry-out of the membrane causes large ionic resistance in the fuel cell. Both of these problems reduce the performance of the PEM fuel cell. The relative humidity (RH) of both the cathode and anode have a significant influence on the water content of the membrane and the condensation of water. Therefore, many studies have investigated the effect of the RH. Some

experimental results have showed that the cell performance increases as the RH increases at relatively low humidity conditions. However, for high humidity conditions, an increase in the RH reduces the performance of the fuel cell as it usually leads to water flooding; see for example (Brett et al., 2007; Santarelli and Torchio, 2007). Also many modelling studies have investigated the effect of the RH and have obtained similar findings; see for example (Kim and Kim, 2016; Xing et al., 2015).

However, all the above studies on the effects of RH were conducted on conventional PEM fuel cells; for air-breathing PEM fuel cells, the number of investigations is less. In air-breathing fuel cells, most of the studies on the effects of the operating conditions focus on the effect of the RH at the open cathode, assuming dry hydrogen is supplied to the anode of the fuel cell; see for example (Zhang et al., 2007). However, there have been very few investigations which have studied the effects of the anodic RH on the performance of the air-breathing PEM fuel cells; most of these investigations were experimental. Chu and Jiang (1999) evaluated the performance of an air-breathing polymer electrolyte membrane fuel cell (PEMFC) stack under different environmental conditions, and they showed that feeding humidified hydrogen to the anode slightly improves the PEMFC performance, even at low temperatures. Ho Jung et al. (2007) examined the effect of the hydrophilicity of the anode catalyst layer on the performance of an air-breathing PEM fuel cell. The experimental results showed that a hydrophilic anode catalyst layer improves the cell performance through humidifying the anode side of the membrane and removing the water from the cathode. Hamel and Fréchette (2011) suggested a simple steady-state model for the water transport through an air-breathing PEM fuel cell and an experimental characterisation was performed with direct injection of water at the anode. They showed that humidifying the anode had a positive effect on the performance of the cell, potentially even when the cathode is flooding. Ou et al. (2017) tested an air-breathing PEM fuel cell with a humidity and temperature control system, and a bubble humidifier was utilized

to humidify the inlet hydrogen in order to manage the water content of the membrane. The experimental results showed that the control method improves the output power of the fuel cell.

To the best of the authors' knowledge, no modelling study has been conducted to investigate the effect of the anodic (hydrogen) RH on the performance of the air-breathing fuel cell. In this study, a mathematical model is built for an air-breathing fuel cell. The effect of the RH of the hydrogen on the cell performance is investigated and compared with that of the RH of ambient air at the open cathode. Also, the effect of the gas diffusion layer (GDL) thickness is examined, since the gas concentrations at the cathode catalyst layer and the membrane humidity condition are highly influenced by the GDL thickness.

2. Numerical model

The prototype of this built model was first described by O'Hayre et al. (2007). A schematic diagram of the modelled fuel cell is shown in Fig.1. As mentioned in our previous study (Ismail et al., 2014), this fuel cell was selected because the temperature of the cathode GDL surface and the cell resistance were measured. Therefore, in addition to the polarisation curves for the cell voltage, further data can be used to validate the proposed new model. The following assumptions have been taken into account when developing the model:

- The fuel cell operates in steady-state conditions.

- The air is treated as an ideal gas.

- The catalyst layer is infinitely thin and is therefore treated as an interface between the membrane and the GDL.

- Water only exits as vapour.

- The GDL material is assumed to be homogenous.

- The fuel cell is under a dead-end mode at the anode side.

- The water activity is uniform across the membrane and is in equilibrium with the water activity at the cathode catalyst layer.

- The thermal resistance of the collectors was found to be almost negligible, therefore the current collectors were not incorporated into the model.

The equations used in the model could be categorised into 3 groups: mass transfer; heat transfer; and closure relations. The equations for each groups are explained below.
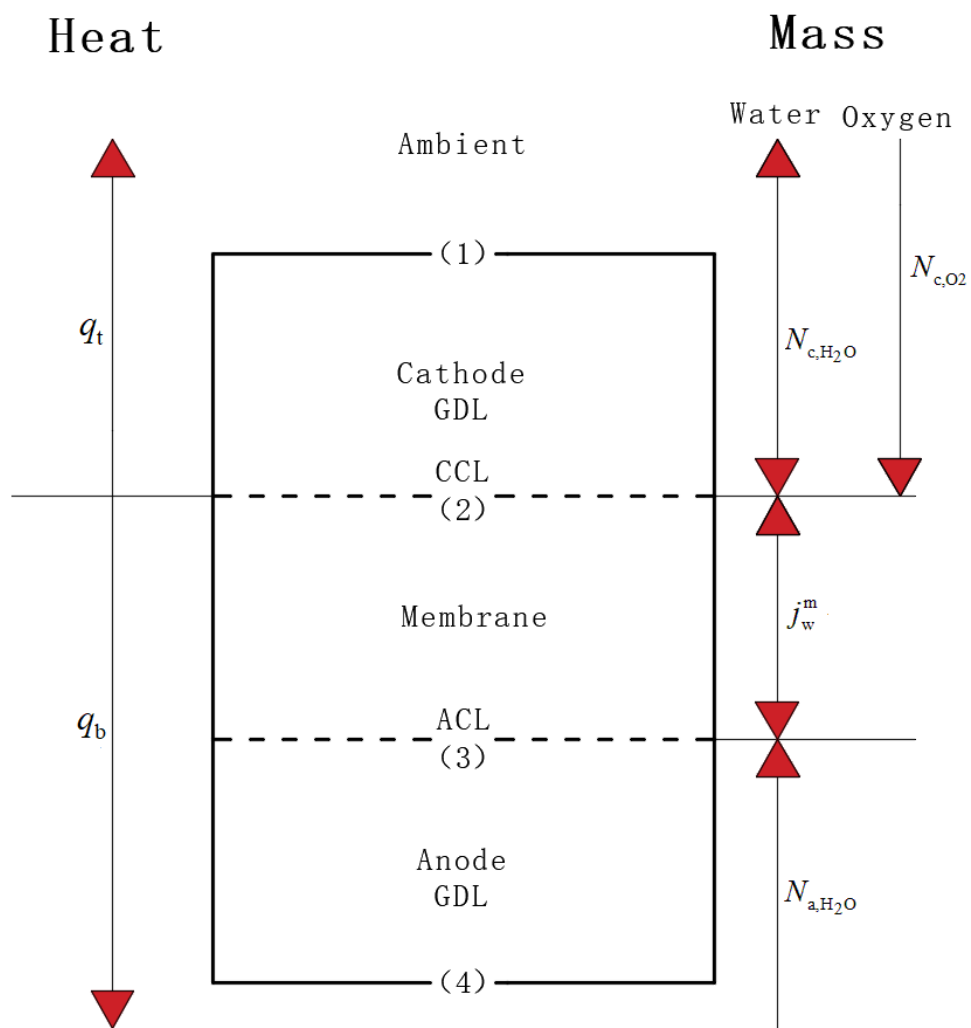

Fig. 1. A schematic diagram of the modelled fuel cell. Each number represents an interface: (1) cathode GDL surface, (2) cathode catalyst layer, (3) anode catalyst layer and (4) anode GDL surface.

2.1.Mass transfer

On the cathode side, oxygen and water are mainly transported by natural convection in the ambient region next to the cathode GDL surface and by diffusion across the GDL. The convective molar flux of the species i in the cathode, i.e. $N_{c,i}$, is given by:

$$N_{c,i} = h_{m,i} (C_{1,i} - C_{\infty,i})$$
(1)

where the subscript i represents either oxygen (O_2) or water (H_2O), $C_{1,i}$ and $C_{\infty,i}$ are the molar concentrations of the species i at the surface of the cathode GDL and in the ambient region next to the cathode GDL, respectively. $h_{m,i}$ is the mass transfer coefficient of the species i and is obtained as follows:

$$h_{m,i} = \frac{Sh_i \cdot D_{ij}}{L_{ch,m}}$$
(2)

D_{ij} is the normal diffusion coefficient of the species i into j; the latter represents nitrogen (N_2). $L_{ch,m}$ is the characteristic length associated with the mass transfer, defined as the square root of the active area of the fuel cell. Sh_i is the Sherwood number, which is associated with the mass transfer, for the species i. It must be noted that the Lewis numbers for all simulation cases were found to be of the order of unity, so the analogy between heat and mass transfers is valid. Another important point to note is that the modelled fuel cell is horizontally-oriented with an upwards-facing open cathode and a uniform wall heat flux (UHF) boundary condition on the surface of the cathode GDL is assumed. Therefore Sh_i is calculated by the following empirical equation (Ghiaasiaan, 2011):

$$Sh_i = 0.16 Ra_{m,i}^{1/3}$$
(3)

The mass transfer-related Rayleigh number $Ra_{m,i}$ for the species i is given by:

$$Ra_{m,i} = \frac{g\beta_{m,i}(x_{1,i} - x_{\infty,i})L_{ch,m}^3}{\nu_i D_{ij}} \quad (4)$$

where g is the magnitude of the gravitational acceleration, ν_i is the kinematic viscosity of the species i, x_i is the mole fraction of the species i, and $\beta_{m,i}$ is the volumetric expansion coefficient of the species i. Since the molar concentration of nitrogen remains almost constant through the cathode GDL and the ambient region, we assume that a binary mixture of oxygen and water is transferred to the open cathode. Thus $\beta_{m,i}$ for the binary mixture is calculated as follows (Ghiaasiaan, 2011):

$$\beta_{m,i} = \frac{M_{O_2} - M_{H_2O}}{M_{mix}} \quad (5)$$

where M_{O_2} and M_{H_2O} are the molecular weights of oxygen and water, respectively, M_{mix} is the molecular weight of the binary mixture and it is the arithmetic mean of the molecular weights of the mixture in the ambient region, $M_{\infty,mix}$, and at the cathode GDL surface, $M_{1,mix}$:

$$M_{mix} = \frac{M_{1,mix} + M_{\infty,mix}}{2} \quad (6)$$

$$M_{\infty,mix} = \frac{C_{\infty,O_2}}{C_{\infty,O_2} + C_{\infty,H_2O}} M_{O_2} + \frac{C_{\infty,H_2O}}{C_{\infty,O_2} + C_{\infty,H_2O}} M_{H_2O} \quad (7)$$

$M_{1,mix}$ can be calculated in the same manner. The molar concentration of the water in the ambient region, C_{∞,H_2O}, is given by:

$$C_{\infty,H_2O} = \frac{P_{sat} RH_\infty}{RT_\infty} \quad (8)$$

where R is the universal gas constant, RH_∞ is the relative humidity in the ambient, T_∞ is the ambient temperature, and P_{sat} is the saturation pressure of water vapour, obtained, in atm units, by the following formula (Springer, 1991):

$$\log_{10} P_{sat} = -2.1794 + 0.02953(T_\infty - 273.15) - 9.1837 \times 10^{-5}(T_\infty - 273.15)^2$$
$$+1.4454 \times 10^{-7}(T_\infty - 273.15)^3 \tag{9}$$

The molar concentration of the oxygen in the ambient region, C_{∞,O_2}, is given by:

$$C_{\infty,O_2} = 0.21(C_{\infty,tot} - C_{\infty,H_2O}) \tag{10}$$

where $C_{\infty,tot}$ is the molar concentration of the air mixture in the ambient region and is given by:

$$C_{\infty,tot} = \frac{P_\infty}{RT_\infty} \tag{11}$$

For the diffusion of water and oxygen across the cathode GDL, $N_{c,i}$ is calculated as follows:

$$N_{c,i} = D_{eff,ij} \frac{C_{2,i} - C_{1,i}}{\delta_{GDL}} \tag{12}$$

where $C_{2,i}$ is the molar concentration of the species i at the cathode catalyst layer, δ_{GDL} is the thickness of the GDL, $D_{eff,ij}$ is the effective diffusion coefficient, and it is obtained as follows (Mench, 2008):

$$D_{eff,ij} = f(\varepsilon)D_{ij}(\frac{T_{GDL}}{T_{ref}})^{1.5}(\frac{P_{ref}}{P}) \tag{13}$$

where T_{ref} and P_{ref} are the reference temperature and pressure, respectively. The pressure ratio (P_{ref} / P) is set to be unity since the operation pressure is the same as the reference pressure, i.e. 1 atm. T_{GDL} is the temperature of the cathode GDL, and is the arithmetic mean of the temperatures at the cathode GDL surface, T_1, and at the cathode catalyst layer, T_2. $f(\varepsilon)$ is the factor that corrects for the geometry and is a function of the porosity of the medium, ε. Instead of using the normally applied Bruggmann correlation, $f(\varepsilon)$ is calculated by a more accurate correlation developed for GDLs (Ismail et al., 2015):

$$f(\varepsilon) = 0.008e^{4.81\varepsilon} \tag{14}$$

At the anode side, water and hydrogen are mainly transported by diffusion across the anode GDL. It should be noted that the concentration of oxygen at the cathode electrode is relatively small due to the low mass transfer coefficient, thus the hydrogen supplied at the anode is usually sufficient for the operation of the air-breathing fuel cell. Thus, the transport of hydrogen is not considered in the model and subsequently the anodic activation losses are neglected. The molar flux of water across the anodic GDL, i.e. N_{a,H_2O}, is given by:

$$N_{a,H_2O} = D_{eff,ij} \frac{C_{4,H_2O} - C_{3,H_2O}}{\delta_{GDL}} \tag{15}$$

Likewise, the effective diffusion coefficient $D_{eff,ij}$ can be calculated using Eq. 13 and Eq. 14. D_{ij} is the normal diffusion coefficient of water vapour into hydrogen as the latter, volume-wise, makes up most of the gas mixture at the anode. C_{3,H_2O} and C_{4,H_2O} are the molar concentrations of water at the anode catalyst layer and at the anode GDL surface. Since the gas mixture at the anode side is treated as an ideal gas, C_{4,H_2O} can be obtained by employing Eq. 8 and Eq. 9.

Water is transported through the membrane through three different processes, namely: water diffusion, electro-osmosis drag and water convection. The diffusion of water is caused by the concentration gradient and this is usually from the cathode to the anode due to the water being produced at the cathode catalyst layer. The electro-osmosis drag occurs because of the conjugated transport of the water molecules with the protons. The convection of water is caused by the pressure gradient (Karpenko-Jereb et al., 2014). Since water only exits as a vapour in this model, water convection is neglected and therefore the total water flux through the membrane from the anode to the cathode is given by (Jiao and Li, 2011):

$$j_w^m = -D_w^m \frac{C_{2,H_2O} - C_{3,H_2O}}{\delta_{mem}} + n_d \frac{I}{F} \tag{16}$$

where I is the current density and F is the Faraday's constant. It should be noted that, for simplification, the catalyst layers are treated as interfaces between the membrane and the GDL and therefore the concentrations of water at the cathode and anode sides of the membrane were assumed to be of those of the cathode and anode catalyst layers respectively, i.e. C_{2,H_2O} and C_{3,H_2O}. The diffusion coefficient, D_w^m, and electro-osmotic drag coefficient, n_d, are dependent on the water content of the membrane, λ, and are given by (Jiao and Li, 2011):

$$D_w^m = \begin{cases} 3.1 \times 10^{-7} \lambda \left[\exp(0.28\lambda) - 1 \right] \exp(-\frac{2346}{T_{mem}}) & \text{if } 0 < \lambda < 3 \\ 4.17 \times 10^{-8} \lambda \left[161 \exp(-\lambda) + 1 \right] \exp(-\frac{2346}{T_{mem}}) & \text{if } 3 \le \lambda < 17 \end{cases} \tag{17}$$

$$n_d = \begin{cases} 1 & \text{if } \lambda \le 14 \\ 0.1875\lambda - 1.625 & \text{otherwise} \end{cases} \tag{18}$$

The water content of the membrane, λ, is calculated by :

$$\lambda = \begin{cases} 0.043 + 17.81a - 39.85a^2 + 36.0a^3 & \text{if } 0 \le a \le 1 \\ 14.0 + 1.4(a-1) & \text{if } 1 < a \le 3 \end{cases} \tag{19}$$

where a is the water activity in the membrane which, as indicated in the assumptions, is assumed to be uniform across the membrane and is in equilibrium with the water activity at the cathode catalyst layer and a is given by:

$$a = \frac{P_{2,H2O}}{P_{2,sat}} \tag{20}$$

where $P_{2,sat}$ is the saturation pressure of the water vapour at the cathode catalyst layer, obtained using Eq. 9, and P_{2,H_2O} is the partial pressure of the water vapour at the cathode catalyst layer,

and is given by:

$$P_{2,H2O} = C_{2,H_2O} R T_2 \tag{21}$$

In the modelled fuel cell, water is transported between the anode and cathode sides of the membrane and also between the ambient and the cathode catalyst layer. It is also produced at the cathode catalyst layer. Thus, the transport of water in the fuel cell, based on Faraday's second law of electrolysis and the model proposed by Berg et al. (2004), is governed by:

$$N_{a,H_2O} = j_w^m \tag{22}$$

for the anode side, and by:

$$N_{c,H_2O} = j_w^m + \frac{I}{2F} \tag{23}$$

for the cathode side. On the other hand, oxygen transports through cathode GDL between the ambient and the cathode catalyst layer and therefore its transport is governed by the following equation:

$$N_{c,O_2} = \frac{I}{4F} \tag{24}$$

2.2. Heat transfer

The heat generated is assumed to be released only from the cathode catalyst layer as most of the heat sources exist. Therefore, the heat is mainly transported by conduction in the GDLs and the membrane; and by natural convection in the ambient region next to the GDL surfaces.

The convective heat flux at the interface between the ambient and the cathode GDL, q_t, is given by:

$$q_t = h_c (T_1 - T_\infty) \tag{25}$$

14

where h_c is the heat transfer coefficient at the surface of the cathode GDL, which is the sum of the natural convection coefficient, $h_{c,con}$, and the radiative coefficient, $h_{c,rad}$:

$$h_c = h_{c,con} + h_{c,rad} \tag{26}$$

$$h_{c,rad} = 2e\sigma_{Bolt}(T_l^2 + T_\infty^2)(T_l + T_\infty) \tag{27}$$

$$h_{c,con} = \frac{Nu_c \cdot k_{c,air}}{L_{ch,h}} \tag{28}$$

where e is the emissivity, σ_{Bolt} is the Stephan-Boltzmann constant, $k_{c,air}$ is the thermal conductivity of air, $L_{ch,h}$ is the characteristic length for heat transfer, and Nu_c is the Nusselt number. As mentioned in the mass transfer section, the fuel cell is assumed to represent a horizontally-oriented heated plate with UHF boundary condition. Nu_c and the relevant Rayleigh number, $Ra_{h,c}$ are then given by (Ghiaasiaan, 2011):

$$Nu_c = 0.16Ra_{h,c}^{1/3} \tag{29}$$

$$Ra_{h,c} = \frac{g\beta_c q_c L_{ch,h}^4}{\nu_{c,air}\alpha_{c,air}k_{c,air}} \tag{30}$$

The kinematic viscosity $\nu_{c,air}$, the thermal diffusivity $\alpha_{c,air}$ and the thermal conductivity $k_{c,air}$ of the air have been all estimated using the tabulated data (Bergman et al., 2011) at the film temperature, $T_{c,f}$, which is the arithmetic mean of the temperatures of the cathode GDL surface, T_l, and the ambient region, T_∞. The thermal expansion coefficient, β_c, is calculated as follows:

$$\beta_c = \frac{1}{T_{c,f}} \tag{31}$$

The convective heat flux at the bottom of the fuel cell, q_b, is calculated in the same manner using Eq. 25 - 31.

With the given thermal conductivities and thicknesses of the GDL and the membrane, i.e. k_{GDL}, δ_{GDL}, k_{mem} and δ_{mem}, The conductive heat fluxes in the GDLs and the membrane are given by:

$$q_t = k_{GDL} \frac{T_2 - T_1}{\delta_{GDL}} \tag{32}$$

$$q_b = k_{mem} \frac{T_2 - T_3}{\delta_{mem}} = k_{GDL} \frac{T_3 - T_4}{\delta_{GDL}} \tag{33}$$

where k_{GDL} and k_{mem} are the thermal conductivities of the GDL and the membrane respectively, and δ_{GDL} and δ_{mem} are the thicknesses of the GDL and the membrane respectively.

2.3. Closure relations

The cell potential E is expressed as follows:

$$E = E_o - \eta_{act} - \eta_{ohmic} \tag{34}$$

where E_o is the thermodynamic equilibrium voltage, η_{act} is the activation loss, and η_{ohmic} is the ohmic loss. It should be noted that the concentration losses, mainly caused by water flooding, has not been considered in this model as the water activity was found to be always less than unity at the high current densities in all the investigated cases, thus signifying the absence of water flooding. The thermodynamic equilibrium voltage E_o is given by the Nernst equation:

$$E_o = \frac{-\Delta H + T\Delta S}{nF} + \frac{RT}{nF} \ln\left(\frac{P_{H_2} \cdot P_{O_2}^{0.5}}{P_{H_2O}} \right) \tag{35}$$

where ΔH and ΔS are the enthalpy and the entropy changes for the fuel cell reaction, respectively. P_{H_2} (1 atm), P_{O_2} (0.21 atm) and P_{H_2O} (usually assumed to be 1 atm) are the partial pressures of hydrogen, oxygen and water under thermodynamic equilibrium. The activation losses, η_{act}, and the ohmic losses, η_{ohmic}, are given by:

$$\eta_{act} = \frac{RT_2}{2\alpha_{ch}F} \ln\left(\frac{C_{\infty,O_2} I}{C_{2,O_2} I_o}\right) \tag{36}$$

$$\eta_{ohmic} = IA(R_{elec} + R_{mem}) \tag{37}$$

where α_{ch} is the charge transfer coefficient, I_o is the reference exchange current density and R_{elec} is the lumped cell resistance of the fuel cell. These three parameters have been obtained from the experimental data (O'Hayre et al., 2007). A is the active area of the fuel cell and R_{mem} is the resistance of the membrane, obtained as follows:

$$R_{mem} = \frac{\delta_{mem}}{A\sigma_{mem}} \tag{38}$$

where σ_{mem} is the ionic conductivity of the membrane. The ionic resistance of the catalyst layer is neglected in the model because two cases where the catalyst layer resistance is included and excluded in the model have been investigated and it is found that the effect of this resistance is negligible. Because the widely-used Springer model (Springer, 1991) for calculating the ionic conductivity of the membrane was found to be rather inaccurate under low humidity conditions, another empirical formula is normally used for the modelled air-breathing fuel cells (Litster and Djilali, 2007):

$$\sigma_{mem} = (3.46a^3 + 0.0161a^2 + 1.42a - 0.175) \times \exp\left[1268\left(\frac{1}{303} - \frac{1}{T_2}\right)\right] \tag{39}$$

The total heat flux in the fuel cell is given by:

$$q = I\left(\eta_{act} + \eta_{ohmic} + \frac{T\Delta S}{2F}\right) = q_t + q_b \tag{40}$$

The simulations in this study were implemented using MATLAB R2017b and the time taken for the convergence using a 3.20 GHz Intel(R) Xeon(R) E3 CPU and 16.00 GB RAM was

remarkably small: 4 s, indicating the efficiency of the developed model. All the physical and geometrical parameters considered in the model are given in Table 1.

Table 1

Values of the parameters applied in the simulations. Unless otherwise stated, the values of the parameters were taken from the experiment data (Ismail et al., 2014; O'Hayre et al., 2007).

Parameter	Value
Faraday's constant, F	96,485 C mol^{-1}
Magnitude of gravitational acceleration, g	9.81 m s^{-2}
Universal gas constant, R	8.314 J mol^{-1} K^{-1}
Stephan-Boltzmann constant, σ_{Bolt}	5.67×10^{-8} W m^{-2} K^{-4}
Enthalpy change of fuel cell reaction, ΔH	-241.98 kJ mol^{-1}
Entropy change of fuel cell reaction, ΔS	-44.43 J mol^{-1} K^{-1}
Diffusivity of oxygen in nitrogen, $D_{O_2-N_2}$	2.2×10^{-5} m^2 s^{-1}
Diffusivity of water vapour in nitrogen, $D_{H_2O-N_2}$	2.56×10^{-5} m^2 s^{-1}
Diffusivity of water vapour in hydrogen, $D_{H_2O-H_2}$	1.02×10^{-4} m^2 s^{-1} (Schwertz and Brow, 1951)
GDL thickness, δ_{GDL}	3.0×10^{-4} m
Membrane thickness, δ_{mem}	5.2×10^{-5} m
GDL thermal conductivity, k_{GDL}	1 W m^{-1} K^{-1}
Membrane conductivity, k_{mem}	0.17 W m^{-1} K^{-1}
GDL porosity, ε	0.4
Emissivity, e	0.9
Active area of fuel cell, A	9.0×10^{-4} m^2
Characteristic length for mass transfer, $L_{ch,m}$	3.0×10^{-2} m
Characteristic length for heat transfer, $L_{ch,h}$	7.0×10^{-2} m
Lumped electrical resistance of the fuel cell, R_{elec}	0.012 Ω
Charge transfer coefficient, α_{ch}	0.41
Reference exchange current density, I_0	3.0×10^{-3} A m^{-2}

3. Results and discussion

To validate the model, the modelling data obtained from the present model are compared with the experimental data reported by (Fabian et al., 2006). It should be noted that although this work was performed some time ago, it is still regarded by many as the benchmark work (Atkinson et al., 2017; Obeisun et al., 2015). Fig. 2(a) shows the polarization curves produced by the model at two ambient temperatures (i.e. 10 and 30°C) and a constant ambient relative

humidity of 40%. One can observe from the figure that the modelling data are in good agreement with the experimental data and that the sharp decline in the cell voltage at high current densities is well captured by the model.

Fig. 2(b) and 2(c) show the cell resistance and the temperature of the cathode GDL surface as a function of the current density for 10 and 30°C ambient temperatures and an ambient relative humidity of 40%. Similarly, good agreement is obtained between the experimental and the modelling data, imparting confidence on the reliability of the model. Further, Fig. 2(a) and 2(b) show that there is a sharp decline in the cell voltage and a steep increase in the cell resistance and these coincide. This means that the cell resistance is the main reason for limiting the air-breathing fuel cell performance at high current densities.
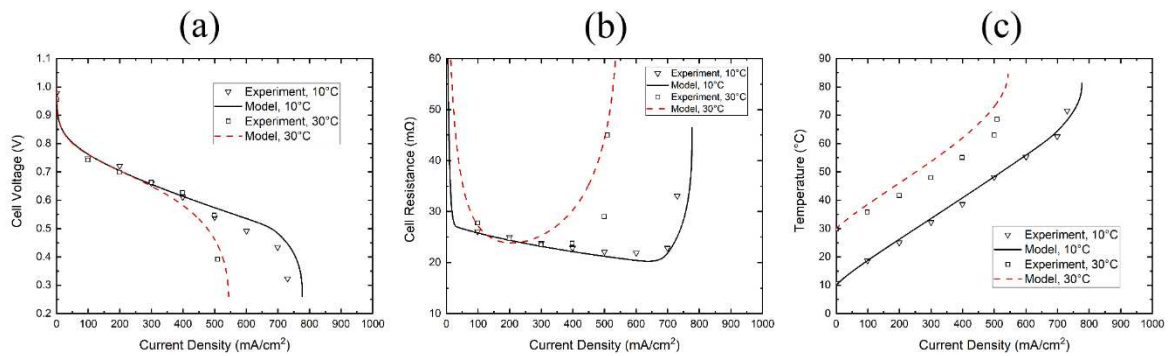

Fig. 2. (a) The cell voltage, (b) cell resistance and (c) GDL surface temperature as a function of the current density for an air-breathing fuel cell operating at 40% ambient relative humidity and ambient temperatures of 10 and 30°C.

3.1. Status of water

It is clear from the previous section that the air-breathing fuel cell is limited mainly by the membrane ohmic resistance at high current densities and thus the performance of the fuel cell increases with decreasing the fuel cell temperature. This must be compared with conventional fuel cells, where the performance is normally limited by water flooding. Therefore, it is of much interest to analyse the status of liquid water at the cathode of the modelled fuel cell; Fig.

3 shows the rates of generation and removal of water (which is equivalent to the water flux at the surface of the cathode GDL), respectively.

Depending upon the relative magnitudes of the water generation and removal rates, the cathode of the fuel cell is said to be under: (i) self-humidification in the low current density region (< 50 mA/cm²) where the difference between the higher rate of water removal and the lower rate of water generation decreases with increasing current density, (ii) water flooding in the intermediate current density region (between 50 and 450 mA/cm²) where the rate of generation of water is always more than the rate of water removal, and (iii) membrane dry-out in the high
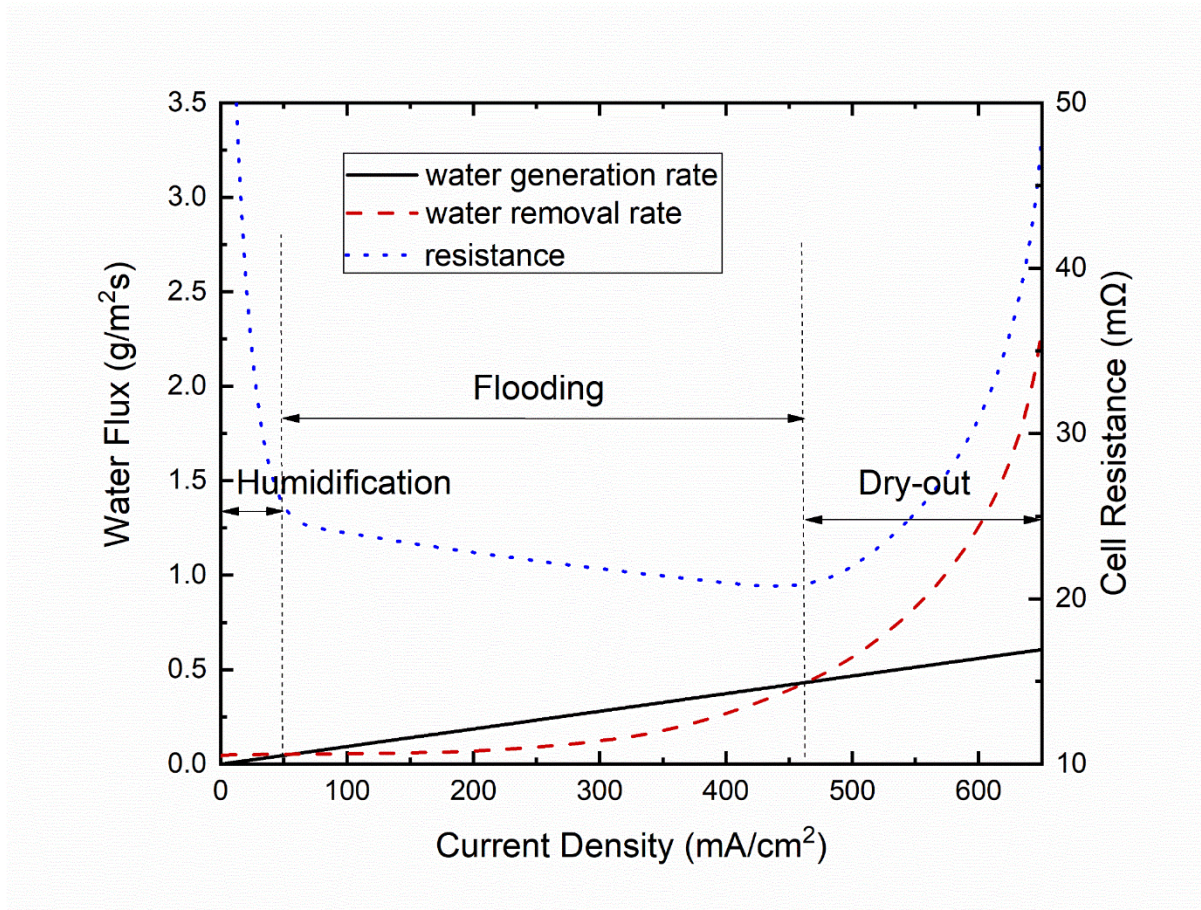
Fig. 3. The water generation rate, the cathode water removal rate and the cell resistance as a function of the current density.

current density region (> 450 mA/cm²) where the rate of water removal is always more than that of water generation and the difference between the two rates increases as the current

density increases. Clearly, fuel cells with such profile, caused by the relatively low heat transfer coefficient, is limited by the dry-out of the membrane, and the higher fuel cell temperature will cause more serious water flooding and thus decrease the fuel cell performance.

In order to determine the sensitivity of the fuel cell performance to the heat transfer coefficient, this coefficient has been increased by a factor of 3. From Fig. 4, it is clear that the cathode of the fuel cell operates under: (i) self-humidification in the low current density region (< 40 mA/cm²) and (ii) water flooding in the current density larger than 40 mA/cm². Unlike the profile shown in Fig. 3, the performance of the fuel cell with higher heat transfer coefficient is limited by water flooding at high current densities which is commonly encountered when operating conventional PEM fuel cells.
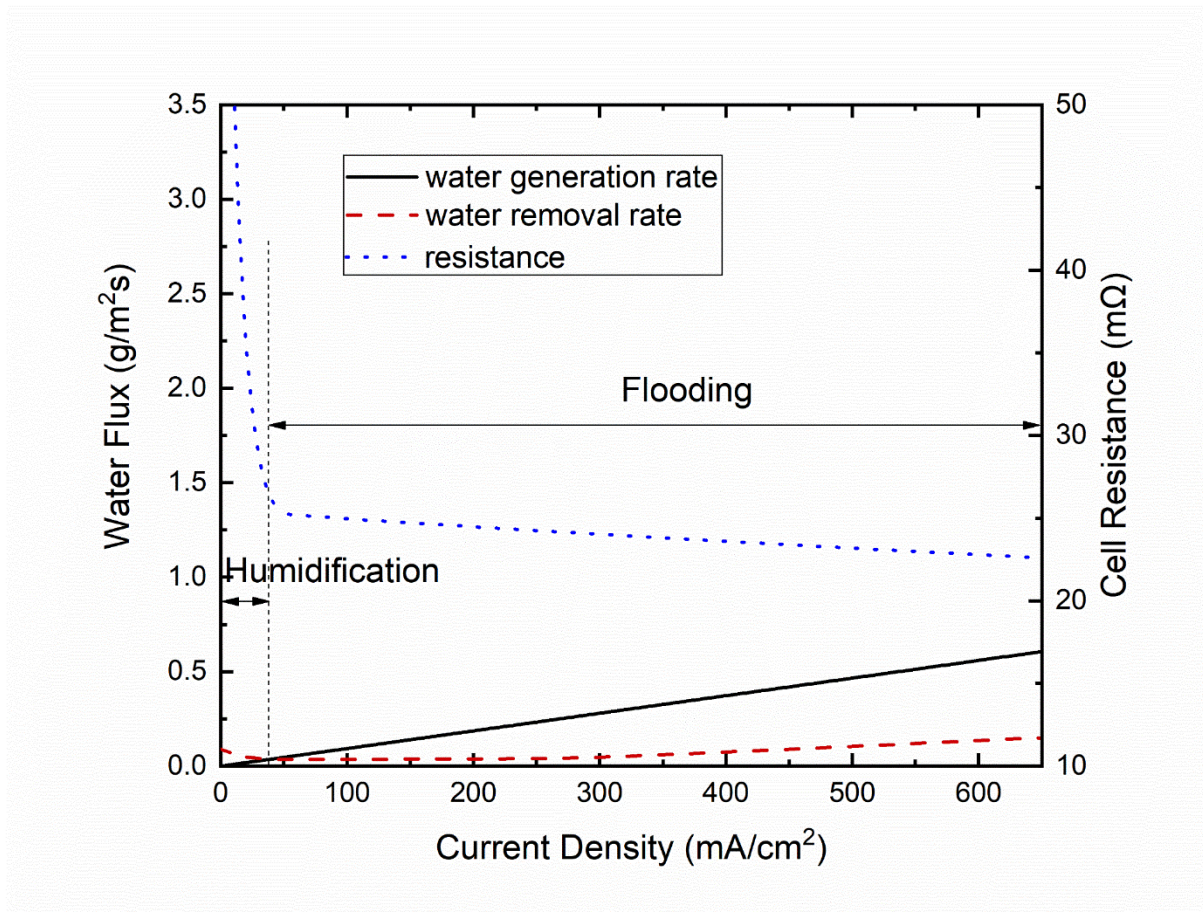

Fig. 4. The water generation rate, the cathode water removal rate and the cell resistance as a function of the current density for the fuel cell with a 3 times larger heat transfer coefficient.

3.2. Effect of anodic humidity

The effect of the humidity at the anode is often neglected when modelling air-breathing PEM fuel cells as hydrogen is normally assumed to be dry. In this section, the effects of both the cathodic relative humidity (or the ambient relative humidity) and the anodic relative humidity on the performance of the air-breathing fuel cell are examined. Figs. 5 and 6 show the effect of the ambient relative humidity. For dry hydrogen (Fig. 5), the cell performance increases slightly with increasing ambient relative humidity, and with fully humidified hydrogen (Fig. 6), the performance gain is even smaller.
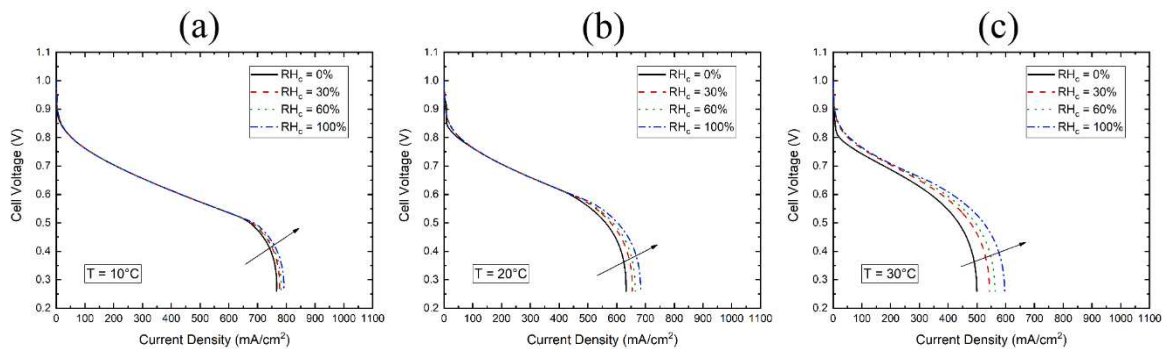

Fig. 5. Effect of the ambient relative humidity at the cathode on the cell performance at zero anodic (hydrogen) relative humidity and three ambient temperatures: (a) 10°C, (b) 20°C and (c) 30°C.
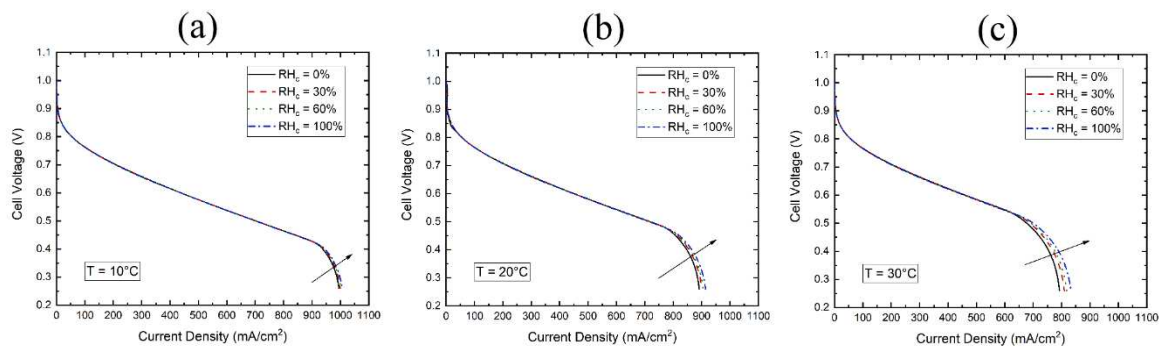

Fig. 6. Effect of the ambient relative humidity at the cathode on the cell performance at 100% anodic (hydrogen) relative humidity and three ambient temperatures: (a) 10°C, (b) 20°C and (c) 30 °C.

Figs. 7 and 8 show the effect of the anodic relative humidity. It is evident that increasing the anode humidity greatly improves the performance of the fuel cell. For example, when the anodic relative humidity increases from 0 to 100% in Fig. 7(c), the limiting current density

increases by more than 40% at 0.3V. Clearly, one of the ways to mitigate membrane dry-out problem at high current density, which has been discussed in Section 3.1, and subsequently enhance the fuel cell performance is to increase the relative humidity of hydrogen.

It also can be seen from Figs. 5 and 7, the performance improvement attributed to the increase in the anodic relative humidity is clearly larger than that attributed to the increase in the ambient relative humidity. Also we can observe that this improvement is only very slightly influenced by the humidity situation at the cathode side (see Figs. 7 and 8). Further, it is observed that for all the cases investigated, the performance improvement is more significant at higher ambient temperatures, and this is due to lower membrane humidification with higher ambient temperatures.
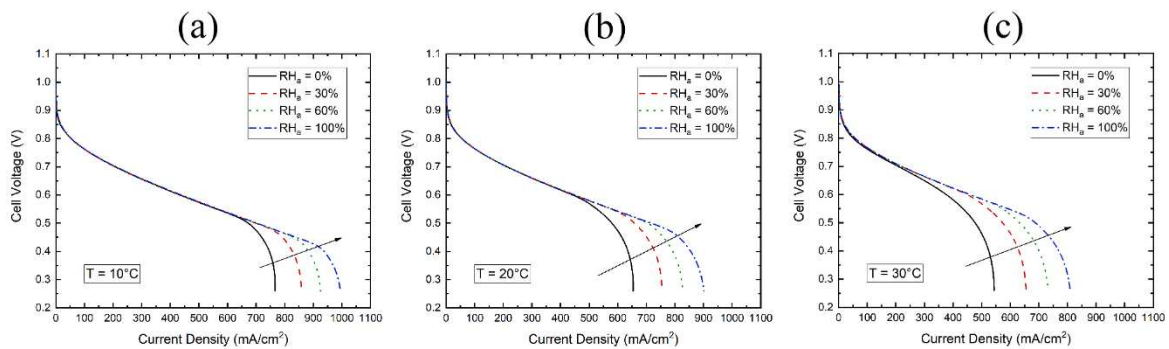

Fig. 7. Effect of the anode (hydrogen) relative humidity on the cell performance at zero cathode relative humidity and three ambient temperatures: (a) 10°C, (b) 20°C and (c) 30°C.
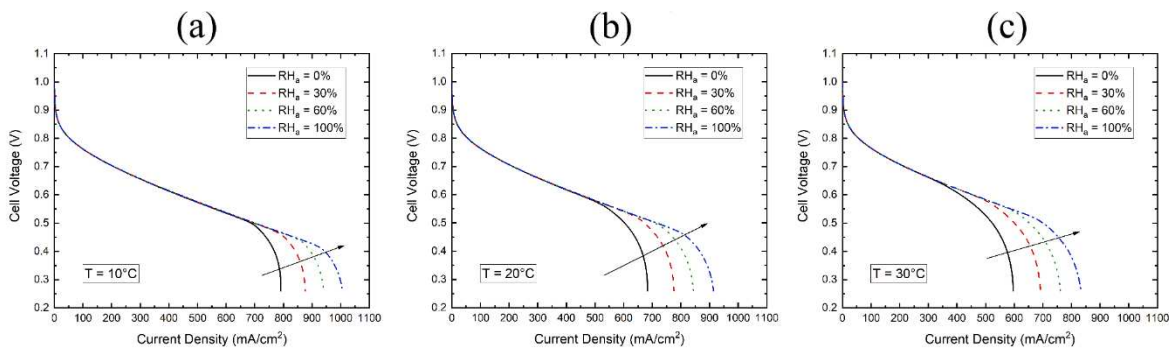

Fig. 8. Effect of the anode (hydrogen) relative humidity on the cell performance at cathode relative humidity) and three ambient temperatures: (a) 10°C, (b) 20°C and (c) 30°C.

23

As mentioned in Section 2, water flooding has not been considered in the model. The increase in both the anode and cathode relative humidity normally cause water flooding at the cathode side of conventional fuel cells particularly at high current densities where the rate of water production is relatively high.

To better understand the effect of the hydrogen relative humidity on water flooding, a figure that shows the accumulating liquid water at the cathode catalyst layer as function of current density is generated; see Fig. 9. For all the investigated cases, the ambient relative humidity and temperature were selected to be 40% and 20°C, respectively, as they are more or less the normal indoor conditions. It should be noted that no temperature control equipment is included in the model, since the air-breathing fuel cell is designed to power small electronic devices where the ancillary components are required to be removed to simplify the system and subsequently boost its competitiveness. It can be seen from the figure that the increase in the relative humidity of hydrogen causes more water to accumulate at the cathode catalyst layer; delaying the occurrence of the limiting current density.

Water activity, which is the ratio between the partial pressure of the water vapour and the saturation pressure of the water vapour, can be also used to confirm whether there exists liquid water. Fig. 10 shows the water activity of the cathode catalyst layer and GDL surface as a function of the anode relative humidity at relatively low cell voltages (i.e. 0.4, 0.3 and 0.2V). Overall, it can be observed that the water activity slightly increases with increasing anodic relative humidity. For example, at 0.4V the water activity of the catalyst layer increases only by 20% when increasing the anodic relative humidity from 0% to 100%. It can be noted that, in all the simulated cases shown in Fig. 10, the water activity is less than unity, and this indicates that no liquid water is produced at the cathode side. Therefore, the increase in the anodic relative humidity does not cause water flooding at high current densities.
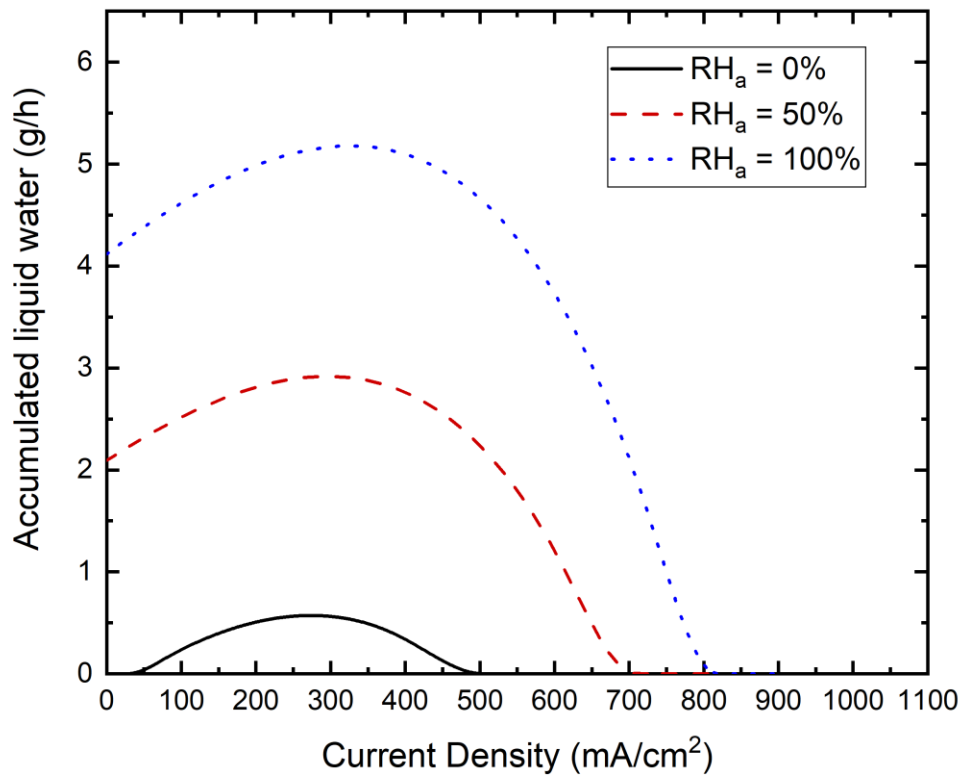
Fig. 9. The accumulating liquid water at the cathode catalyst layer as a function of the current density for the fuel cell operating at different anode (hydrogen) relative humidities.
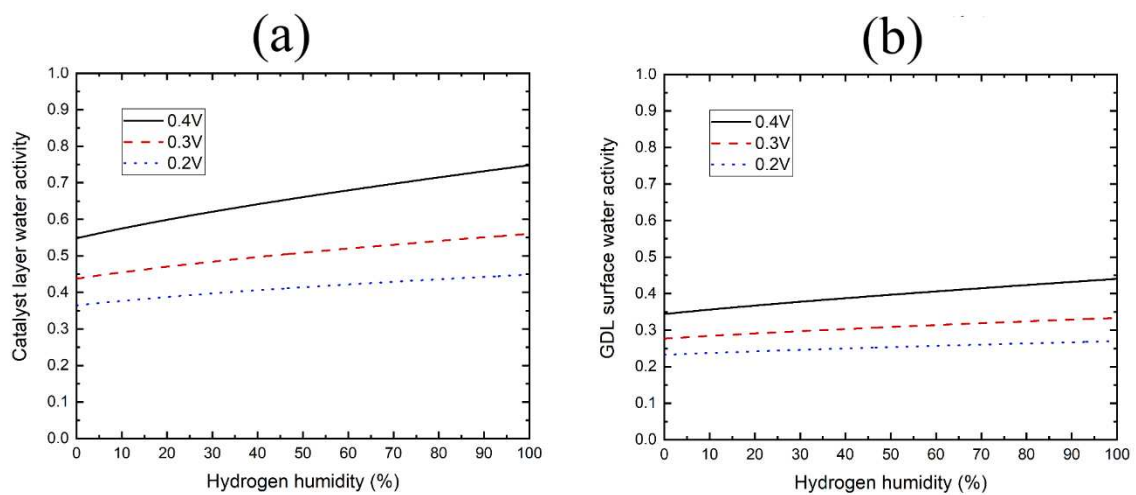

Fig. 10. Effect of anodic (hydrogen) relative humidity on the water activity at relatively low cell voltages and at (a) cathode catalyst layer and (b) cathode GDL surface.

3.3. Effect of GDL thickness

The results presented in Section 3.2 show that the increase in the anodic relative humidity improves the performance of the air-breathing fuel cell by increasing the water vapour concentration at the cathode catalyst layer and subsequently its ionic conductivity. Also, the variation of GDL thickness can influence the diffusion of the water vapour at the cathode and thus change the water vapour concentration. For dry and fully humidified hydrogen, the effects of GDL thickness on the cell performance are investigated.

It can be seen that, from Fig. 11, the most appropriate GDL thickness, at either the cathode or anode, for operation of the air-breathing fuel cell is different at two humidity conditions at the anode side. For the dry condition, a thicker GDL is favoured, e.g. 0.8 mm thickness; see Fig. 11(a). While for the fully humidified condition, the cell performs better with a thinner GDL, i.e. 0.2 mm thickness; see Fig. 11(b). The thickness of the GDL mainly influences the diffusion of the water vapour and oxygen. The cell performance is largely dependent on the concentrations of these two gases and therefore it is necessary to investigate the relationships between these concentrations and the GDL thickness.
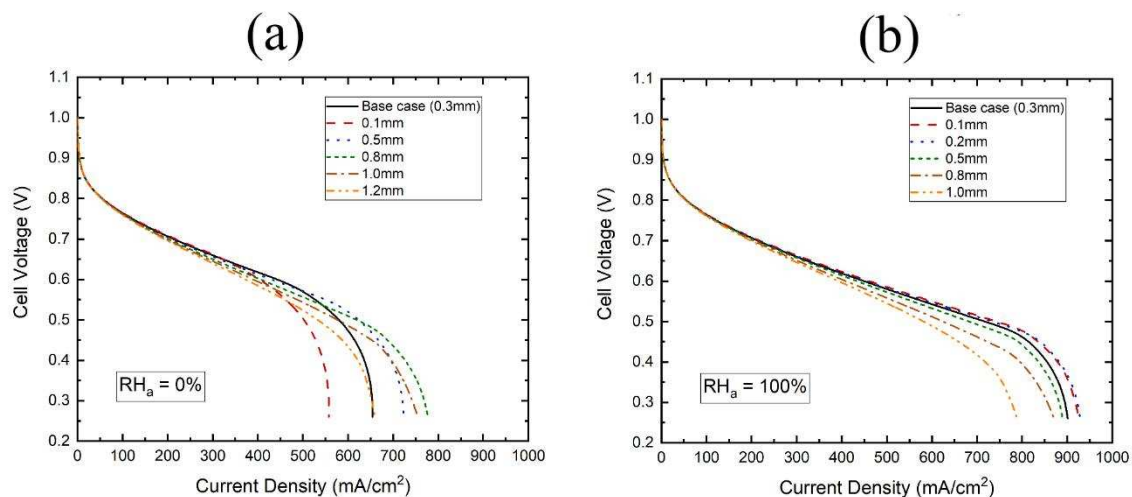

Fig. 11. Effect of the GDL thickness on the cell performance at two anodic (hydrogen) relative humidity: (a) 0% and (b) 100%.

Fig. 12 shows the effect of the GDL thickness on the gas concentrations at 0.4V and at two humidity conditions. For the dry condition (Fig. 12(a)), we can observe that the GDL thickness has opposite effect on the concentrations of water and oxygen. This is because, at the fuel cell cathode side, the water is transported from where it is produced at the cathode catalyst layer towards the ambient, while oxygen is transported in the opposite direction, i.e. from the ambient to where it is consumed at the cathode catalyst layer. When a thicker GDL is chosen, it becomes more difficult for water to be transported from the cathode catalyst layer to the ambient region and for oxygen to be transported from the ambient to the catalyst layer. For this reason, an optimal thickness is favoured to ensure the supply of sufficient oxygen for the oxygen reduction reaction and to supply sufficient water vapour to appropriately humidify the membrane. However for the fully humidified condition (Fig. 12(b)), water vapour is also transported from the anode side to the cathode catalyst layer. Thus a thinner GDL at the anode side enhances the diffusion of water vapour through the GDL, thus causing the water concentration to reach a relatively high value, and then it follows the same trend as the dry condition. For this case, a thinner GDL is appropriate for the cell operation at the high humidified conditions since there is a relatively high concentration of water and oxygen at the
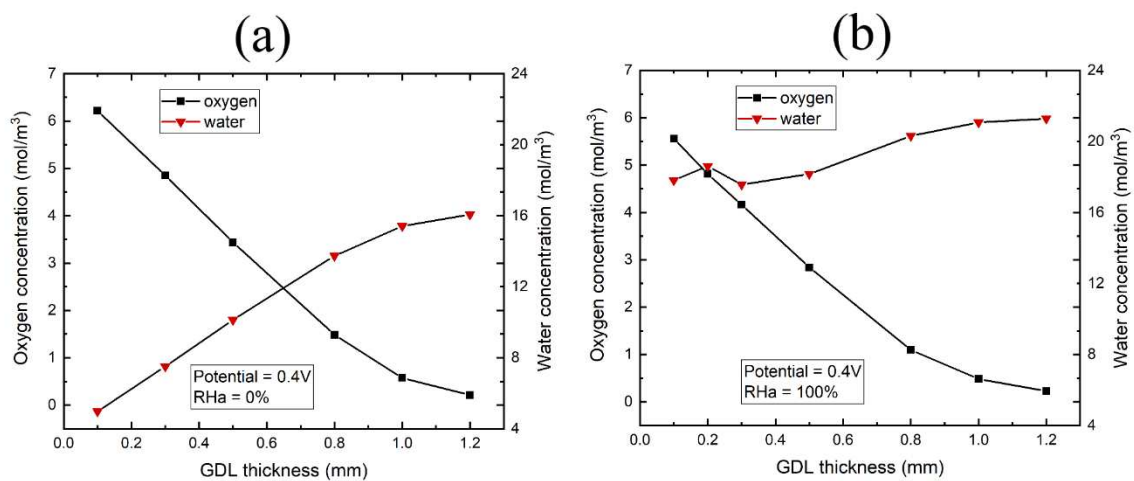

Fig. 12. Effect of the GDL thickness on the oxygen and water vapour as the cathode catalyst layer at two anode (hydrogen) relative humidity: (a) 0% and (b) 100%.

cathode catalyst layer.

Based on the above findings, it could be stated that there exists an optimal thickness for the cathode GDL that ensures sufficient supply of both oxygen and water vapour. On the other hand, a relatively thin GDL can improve the transfer of water vapour to the cathode and this improvement becomes more profound as hydrogen relative humidity increases.

It should be noted that a relatively thick GDL can cause water flooding; Fig. 13 shows that relatively thick GDLs (i.e. 0.8 and 1.2 mm) causes water activity to be more than unity for most of the anodic relative humidity values, thus leading to possible water flooding.
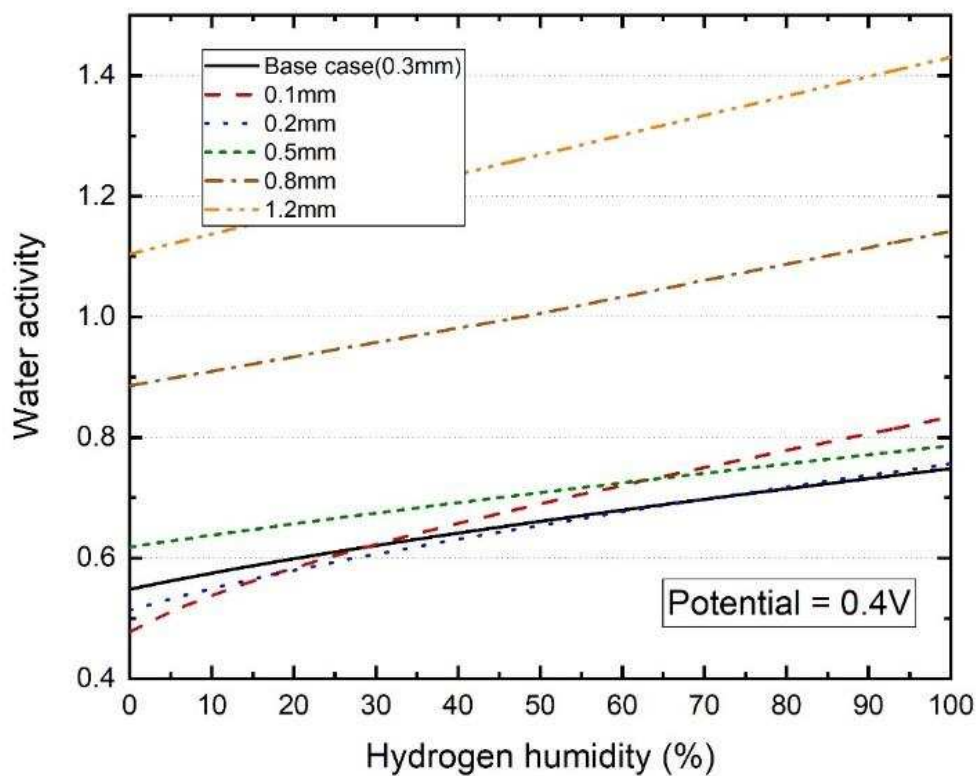

Fig. 13. Effect of the GDL thickness on the water activity at the cathode catalyst layer.

4. Conclusions

A mathematical zero-dimensional model has been developed for air-breathing PEM fuel cells. The main purpose of this study is to examine the effects of hydrogen humidity on the performance of air-breathing PEM fuel cells. The main conclusions are as follows:

- The heat transfer coefficient dictates the performance limiting mode of the air-breathing PEM fuel cell: dry-out of the membrane with relatively low heat transfer coefficient and water flooding with relatively high heat transfer coefficient.

- The performance of the fuel cell significantly improves with increasing anodic (hydrogen) relative humidity and this is due to the increase in the water concentration at the cathode catalyst layer at high current densities. For example, the limiting current density increases by more than 40% at an ambient temperature of 30 °C when increasing the anodic relative humidity from 0 to 100%. This improvement is marginally influenced by the humidity condition at the cathode side. Further, the increase in the anodic relative humidity does not cause water flooding at high current densities.

- In order to maintain high concentrations of both oxygen and water vapour at the cathode catalyst layer, there is an optimal thickness for the cathode GDL. However, for anode GDLs, the thinner GDLs are preferred to enhance the diffusion of water vapour at the anode and consequently increase the water concentration at the cathode, and this improvement is more significant with the hydrogen relative humidity increases.

References

Atkinson, R.W., Hazard, M.W., Rodgers, J.A., Stroman, R.O. and Gould, B.D. (2017), "An Open-Cathode Fuel Cell for Atmospheric Flight", Journal of The Electrochemical Society, Vol. 164 No. 2, pp. F46–F54.

Berg, P., Promislow, K., St. Pierre, J., Stumper, J. and Wetton, B. (2004), "Water Management in PEM Fuel Cells", Journal of The Electrochemical Society, Vol. 151 No. 3, p. A341.

Bergman, T.L., Lavine, A.S., Incropera, F.P. and DeWitt, D.P. (2011), Introduction to Heat Transfer, John Wiley & Sons, Inc., New York.

Brett, D.J.L., Atkins, S., Brandon, N.P., Vasileiadis, N., Vesovic, V. and Kucernak, A.R. (2007), "Membrane resistance and current distribution measurements under various operating conditions in a polymer electrolyte fuel cell", Journal of Power Sources, Vol. 172 No. 1, pp. 2–13.

Carcadea, E., Ene, H., Ingham, D.B., Lazar, R., Ma, L., Pourkashanian, M. and Stefanescu, I. (2007), "A computational fluid dynamics analysis of a PEM fuel cell system for power generation", edited by Bennacer, R.International Journal of Numerical Methods for Heat & Fluid Flow, Vol. 17 No. 3, pp. 302–312.

Chu, D. and Jiang, R. (1999), "Performance of polymer electrolyte membrane fuel cell (PEMFC) stacks Part I. Evaluation and simulation of an air-breathing PEMFC stack", Journal of Power Sources, Vol. 83 No. 1–2, pp. 128–133.

Coz, E., Théry, J., Boillat, P., Faucheux, V., Alincant, D., Capron, P. and Gébel, G. (2016), "Water management in a planar air-breathing fuel cell array using operando neutron imaging", Journal of Power Sources, Vol. 331, pp. 535–543.

Fabian, T., O'Hayre, R., Litster, S., Prinz, F.B. and Santiago, J.G. (2010), "Active water management at the cathode of a planar air-breathing polymer electrolyte membrane fuel cell using an electroosmotic pump", Journal of Power Sources, Elsevier B.V., Vol. 195 No. 11, pp. 3640–3644.

Fabian, T., Posner, J.D., O'Hayre, R., Cha, S.W., Eaton, J.K., Prinz, F.B. and Santiago, J.G. (2006), "The role of ambient conditions on the performance of a planar, air-breathing hydrogen PEM fuel cell", Journal of Power Sources, Vol. 161 No. 1, pp. 168–182.

Ghiaasiaan, M. (2011), Convective Heat and Mass Transfer, Cambridge University Press, Cambridge, available at:https://doi.org/10.1017/CBO9780511800603.

Hamel, S. and Fréchette, L.G. (2011), "Critical importance of humidification of the anode in miniature air-breathing polymer electrolyte membrane fuel cells", Journal of Power Sources, Elsevier B.V., Vol. 196 No. 15, pp. 6242–6248.

Ho Jung, U., Uk Jeong, S., Tae Park, K., Mee Lee, H., Chun, K., Woong Choi, D. and Kim, S.H. (2007), "Improvement of water management in air-breathing and air-blowing PEMFC at low temperature using hydrophilic silica nano-particles", International Journal of Hydrogen Energy, Vol. 32 No. 17, pp. 4459–4465.

Ismail, M., Ingham, D., Hughes, K.J., Ma, L. and Pourkashanian, M. (2016), "The effects of shape on the performance of cathode catalyst agglomerates in polymer electrolyte fuel cells", International Journal of Numerical Methods for Heat & Fluid Flow, Vol. 26 No. 3/4, pp. 1145–1156.

Ismail, M.S., Ingham, D.B., Hughes, K.J., Ma, L. and Pourkashanian, M. (2013), "Thermal modelling of the cathode in air-breathing PEM fuel cells", Applied Energy, Vol. 111, pp. 529–537.

Ismail, M.S., Ingham, D.B., Hughes, K.J., Ma, L. and Pourkashanian, M. (2014), "An efficient mathematical model for air-breathing PEM fuel cells", Applied Energy, Vol. 135, pp. 490–503.

Ismail, M.S., Ingham, D.B., Hughes, K.J., Ma, L. and Pourkashanian, M. (2015), "Effective diffusivity of polymer electrolyte fuel cell gas diffusion layers: An overview and numerical study", International Journal of Hydrogen Energy, Vol. 40 No. 34, pp. 10994–11010.

Jeong, S.U., Cho, E.A., Kim, H.J., Lim, T.H., Oh, I.H. and Kim, S.H. (2006), "Effects of cathode open area and relative humidity on the performance of air-breathing polymer electrolyte membrane fuel cells", Journal of Power Sources, Vol. 158 No. 1, pp. 348–353.

Jiao, K. and Li, X. (2011), "Water transport in polymer electrolyte membrane fuel cells", Progress in Energy and Combustion Science, Elsevier Ltd, Vol. 37 No. 3, pp. 221–291.

Karpenko-Jereb, L., Innerwinkler, P., Kelterer, A.M., Sternig, C., Fink, C., Prenninger, P. and Tatschl, R. (2014), "A novel membrane transport model for polymer electrolyte fuel cell simulations", International Journal of Hydrogen Energy, Elsevier Ltd, Vol. 39 No. 13, pp. 7077–7088.

Kim, H.Y. and Kim, K. (2016), "Numerical study on the effects of gas humidity on proton-exchange membrane fuel cell performance", International Journal of Hydrogen Energy, Elsevier Ltd, Vol. 41 No. 27, pp. 11776–11783.

Li, S. and Ake Sunden, B. (2018), "Numerical analysis on thermal performance of cooling plates with wavy channels in PEM fuel cells", International Journal of Numerical Methods for Heat & Fluid Flow, Vol. 28 No. 7, pp. 1684–1697.

Litster, S. and Djilali, N. (2007), "Mathematical modelling of ambient air-breathing fuel cells for portable devices", Electrochimica Acta, Vol. 52 No. 11, pp. 3849–3862.

Mahmud Hasan, A.B., Wahab, M.A. and Guo, S.M. (2011), "CFD analysis of a PEM fuel cell for liquid dispersion at the interface of GDL-GFC", International Journal of Numerical Methods for Heat & Fluid Flow, Vol. 21 No. 7, pp. 810–821.

Mench, M.M. (Ed.). (2008), Fuel Cell Engines, John Wiley & Sons, Inc., Hoboken, NJ, USA, available at:https://doi.org/10.1002/9780470209769.

O'Hayre, R., Fabian, T., Litster, S., Prinz, F.B. and Santiago, J.G. (2007), "Engineering model of a passive planar air breathing fuel cell cathode", Journal of Power Sources, Vol. 167 No. 1, pp. 118–129.

Obeisun, O.A., Meyer, Q., Engebretsen, E., Finegan, D.P., Robinson, J.B., Hinds, G., Shearing, P.R., et al. (2015), "Study of water accumulation dynamics in the channels of an open-cathode fuel cell through electro-thermal characterisation and droplet visualisation", International Journal of Hydrogen Energy, Elsevier, Vol. 40 No. 46, pp. 16786–16796.

Ou, K., Yuan, W.W., Choi, M., Yang, S. and Kim, Y.B. (2017), "Performance increase for an open-cathode PEM fuel cell with humidity and temperature control", International Journal of Hydrogen Energy, Elsevier Ltd, Vol. 42 No. 50, pp. 29852–29862.

Santarelli, M.G. and Torchio, M.F. (2007), "Experimental analysis of the effects of the operating variables on the performance of a single PEMFC", Energy Conversion and Management, Vol. 48 No. 1, pp. 40–51.

Schmitz, A., Tranitz, M., Eccarius, S., Weil, A. and Hebling, C. (2006), "Influence of cathode opening size and wetting properties of diffusion layers on the performance of air-breathing PEMFCs", Journal of Power Sources, Vol. 154 No. 2, pp. 437–447.

Schwertz, F.A. and Brow, J.E. (1951), "Diffusivity of water vapor in some common gases", The Journal of Chemical Physics, Vol. 19 No. 5, pp. 640–646.

Springer, T.E. (1991), "Polymer Electrolyte Fuel Cell Model", Journal of The Electrochemical Society, Vol. 138 No. 8, p. 2334.

Xing, L., Das, P.K., Song, X., Mamlouk, M. and Scott, K. (2015), "Numerical analysis of the optimum membrane/ionomer water content of PEMFCs: The interaction of Nafion® ionomer content and cathode relative humidity", Applied Energy, Elsevier Ltd, Vol. 138, pp. 242–257.

Zhang, Y., Mawardi, A. and Pitchumani, R. (2007), "Numerical studies on an air-breathing proton exchange membrane (PEM) fuel cell stack", Journal of Power Sources, Vol. 173 No. 1, pp. 264–276.